Pulmonary Lobe Segmentation in CT Images using Alpha-Expansion

Nicola Giuliani[1], Christian Payer[2], Michael Pienn[1], Horst Olschewski[3] and Martin Urschler[2,4]

[1]*Ludwig Boltzmann Institute for Lung Vascular Research, Graz, Austria*

[2]*Institute of Computer Graphics and Vision, Graz University of Technology, Graz, Austria*

[3]*Department of Pulmonology, Medical University of Graz, Graz, Austria*

[4]*Ludwig Boltzmann Institute for Clinical Forensic Imaging, Graz, Austria*

Keywords: Lung Lobe Segmentation, Discrete Optimization, Graph Cuts, Alpha-Expansion.

Abstract: Fully-automatic lung lobe segmentation in pathological lungs is still a challenging task. A new approach for automatic lung lobe segmentation is presented based on airways, vessels, fissures and prior knowledge on lobar shape. The anatomical information and prior knowledge are combined into an energy equation, which is minimized via graph cuts to yield an optimal segmentation. The algorithm is quantitatively validated on an in-house dataset of 25 scans and on the LObe and Lung Analysis 2011 (LOLA11) dataset, which contains a range of different challenging lungs (total of 55) with respect to lobe segmentation. Both experiments achieved solid results including a median absolute distance from manually set fissure markers of 1.04mm (interquartile range: 0.88-1.09mm) on the in-house dataset and a score of 0.866 on the LOLA11 dataset. We conclude that our proposed method is robust even in case of pathologies.

1 INTRODUCTION

Lung lobe segmentation from thoracic computed tomography (CT) images is a promising method to replace invasive methods for the quantification and localisation of parenchymal destruction in lung diseases (Bragman et al., 2017). This is of particular interest in Chronic Obstructive Pulmonary Disease (COPD) (Tanabe et al., 2012) (Weder et al., 1997). There, computer-aided diagnosis algorithms can be used for the detection and grading of emphysematous changes and the evaluation of fissure integrity. The former can aid in establishing a patient's need for lung volume reduction surgery and the latter can identify patients who can benefit from valve-based lung volume reduction (Schuhmann et al., 2015).

The human lung is divided into five lobes by tree fissures, invaginations of visceral pleura extending from the periphery of the lungs to the hilum (Hayashi et al., 2001). The right lung is separated into three lobes by two fissures, the oblique and the horizontal fissure. The left lung is divided into two lobes by the oblique fissure. Typically the fissures are a double-layer of visceral pleura devoid of vascular structures and airways, however, there is a substantial variation in the general population (Aziz et al., 2004).

In thoracic CT images, the fissures appear as bright planar structures. However, their thin and variable structure in combination with image noise, blurring due to patient movement, and inhomogeneous intensity values make them hard to detect with automatic algorithms. Additional challenges are posed by vessels and bronchi running in close proximity and by pathological deformations of the fissure by adjacent lung tissue. Developmental failure or pathologic processes may even cause the absence of complete fissures (Hayashi et al., 2001).

This creates a need for computer algorithms capable of identifying fissures where they are visible on the thoracic CT images and extrapolate to plausible lobe boundaries in regions where they are not. Several approaches have been proposed besides the semiautomatic methods (Lassen-Schmidt et al., 2017). Some methods are based on using information on lobar shape i.e. learning an atlas and fitting the atlas to potential incomplete fissures (Zhang et al., 2006). Whereas others are using anatomical information of the lung such as the airway and vascular trees to interpolate a boundary in regions where no fissures are detected (Van Rikxoort et al., 2010) (Doel et al., 2012).

As (Doel et al., 2015) have pointed out, both approaches have advantages and disadvantages and

387

the presented methods face problems with pathological lungs, which makes pulmonary lobe segmentation still a challenging task and an active area of research.

In this work, we propose a method that allows to use both anatomical structures as well as prior knowledge on the shape of lobes. To that end we combine information from anatomical lung structures such as the airways, vessels and fissures with prior knowledge on the appearance of the lobes in form of the Potts model into an energy equation. Furthermore, the fissure segmentation step of (Lassen et al., 2013) is improved by extending it to a multiscale approach. This leads to an increase of detected fissures, which is especially of importance in cases where they are pathologically thick. Minimizing this energy equation via $\alpha-$expansion is consequently yielding an optimal lung lobe segmentation.

Up to our knowledge, we are the first to incorporate anatomical structures into a multi-label graph cut segmentation for lung lobe segmentation and show promising results following this approach.

2 METHODS

We present a method for pulmonary lobe segmentation based on minimizing an energy equation via graph cuts. The aim of our study was to develop the aforementioned energy equation, which takes anatomical structures and prior knowledge about the shape of lung lobes into account. Figure 1 shows an overview of the algorithm. First the airway tree and the lungs are segmented. After separating the lungs into left and right lung, a segmentation of the vessel trees is performed for each side. The fissures are segmented in the next step by considering the vessel trees. In the final step of the algorithm all lung structures are combined in an energy equation, which is then minimized using the α-expansion algorithm (Boykov et al., 2001). The result is a 3D volume where each voxel is assigned to one of five labels corresponding to the lobes.

2.1 Computing Lung Structures

In this section the computation of the airway, lung, vessel and fissure segmentation is described.

2.1.1 Airways

The airway segmentation is a combination of two algorithms. Using the first approach, initially a point inside the trachea is detected by scanning for a dark circle in the top-most slices. Starting from this point,

an iterative 3D-region growing algorithm is applied to segment the airways (Helmberger et al., 2014). The second airway segmentation is obtained by using the PartialLungLabelMapImageFilter from the Chest Imaging Platform (San Jose Estepar et al., 2015). As each algorithm has its own strengths and performs better in different cases they are combined to obtain more stable results.

After obtaining an airway segmentation the branches of the airway are labelled corresponding to the lung lobes. In order to achieve this, the segmentation first has to be skeletonized. Based on the anatomical structure of the airway tree it is now possible to label the branches. This is done similar to the method presented in (Gu et al., 2012). First an undirected acyclic graph is extracted from the airway skeleton. Starting from a root vertex at the trachea the next branching point is found by looking for a vertex with three neighbors. Having found the carina it is now possible to separate the airway into left and right lung. The left lung can easily be divided into upper and lower lobe by finding the next branching point and comparing the coordinates of the branches' end points. In the right lung the same approach is used for three lobes.

2.1.2 Lungs

Similar to the airway segmentation, the lung segmentation is a combination of two algorithms. First the lung is segmented following a grey-level thresholding (Otsu, 1979) approach with subsequent morphological closing operations. In cases where this approach fails the PartialLungLabelMapImageFilter from the Chest Imaging Platform (San Jose Estepar et al., 2015) is used.

With the help of the labelled airway segmentation, the lung can now be separated into left and right lung.

2.1.3 Vessels

The algorithm by (Payer et al., 2016) is used for the vessel segmentation. It is first enhancing vascular structures with a multiscale tubularity filter (Law and Chung, 2008). Vessel paths are generated by identifying regularly spaced local maxima in the vessel enhanced images, which are connected to four-dimensional tubular paths (Benmansour et al., 2013). In the resulting local maxima graph a path for each edge between its two end points is extracted that minimizes the geodesic distance. The tubular paths are then filtered and grouped together to distinct vascular subtrees. As we are not interested in knowing which vessel is an artery or vein, the algorithm is stopped at this point.
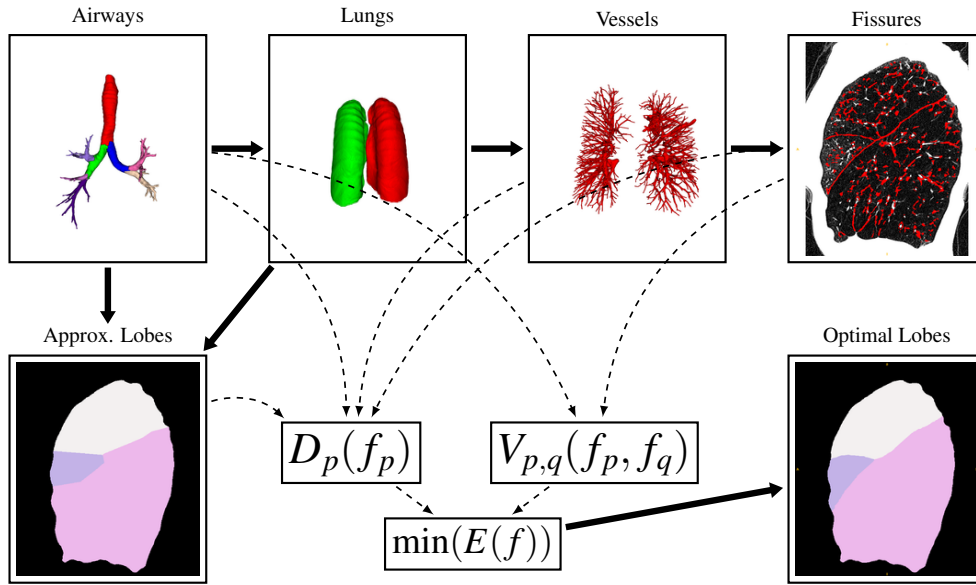
Figure 1: Overview of the segmentation pipeline. The airways, lungs, vessels and fissures are computed subsequently. The airway segmentation is used to obtain an approximate lung lobe segmentation. All lung structures and the approximate segmentation are then combined in an energy equation, which, leads to the optimal 3D lung lobe segmentation after minimization.

2.1.4 Fissures

Pulmonary fissures appear as sheet-like structures in CT scans. Based on an eigenvalue analysis of the Hessian matrix $\mathbf{H}$, voxels that are part of a sheet-like structure are enhanced. The eigenvalues of the Hessian matrix are defined as $|\lambda_1| \leq |\lambda_2| \leq |\lambda_3|$. In (Lassen et al., 2013) the authors proposed a fissure similarity measure $S_{Fissure}$, which combines two features $F_{Structure}$ and F_{Sheet}:

$$S_{Fissure} = F_{Structure} \cdot F_{Sheet} \qquad (1)$$

$$F_{Structure} = \theta(-\lambda_3)e^{\frac{-(\lambda_3-\alpha)^6}{\beta^6}} \qquad (2)$$

$$F_{Sheet} = e^{\frac{-\lambda_2^6}{\gamma^6}} \qquad (3)$$

$F_{Structure}$ is used for finding structure in the image. The parameters α and β in (2) are set to 50 and 35 respectively. As fissures appear as bright structures on a dark background the Heavyside function θ ensures that voxels with an eigenvalue of $\lambda_3 \geq 0$ are not considered as fissures. F_{Sheet} is used to capture sheet-like structures. Vessels have larger λ_2 values than fissures and are thus suppressed by this term. The parameter γ is set to 25. The values for the presented parameters were chosen according to the empirical analysis presented in (Lassen et al., 2013).

A mask of potential fissure voxels M_C is constructed by computing $S_{Fissure}$ for every voxel in the image and by only keeping those voxels that satisfy $S_{Fissure} >$

0.1. M_C is then filtered by a 3D-vector-based connected component analysis with a 6-neighborhood. In case of a sheet the eigenvector corresponding to λ_3 points perpendicular to the direction of the structure. This property is used to measure the similarity of adjacent voxels by calculating the inner product of the normalized eigenvectors of neighboring voxels. Two neighboring voxels are considered as connected, if the aforementioned inner product is larger or equal than 0.98. All components that are smaller than a threshold are then rejected.

For the computation of $\mathbf{H}$ the differentiation is defined as a convolution with derivatives of Gaussians (Frangi et al., 1998). In (Lassen et al., 2013) the computation was done with $\sigma = 1.0$mm. In cases of pathological lungs it often occurs that fissures are significantly larger than in healthy lungs. Empirical analysis showed that $\mathbf{H}$ computed with $\sigma = 1.0$ was often too low to capture thick fissures. As our energy equation in (4) is fairly robust against false positives concerning fissures, we favoured computing the fissure segmentation on multiple scales for σ in the range of $[0.5 - 2.0]$. This range has empirically shown to detect fissures to a great extent on a variety of CT datasets. These results on multiple scales are then combined into a single image F_{MS}. The drawback of increasing σ to large values up to 2.0mm can lead to a lot of vessels being falsely detected as fissures. To circumvent this problem, the previously computed vessel segmentation is dilated and subtracted from the multiscale fissure segmentation F_{MS}. Figure 2 on the
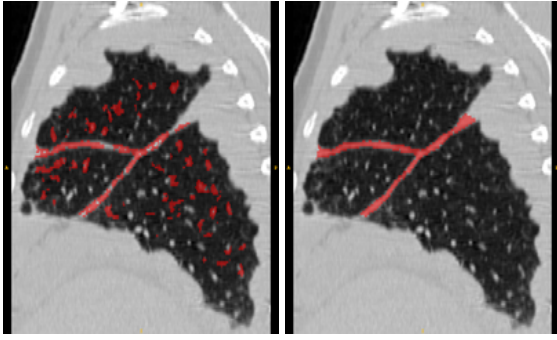
Figure 2: Left: Example for a fissure segmentation result of a right lung with pathological thick fissures. While the fissures are almost fully segmented, the result also contains falsely detected structures. Right: A reference standard, in which the fissures are fully segmented.

left shows a multiscale fissure segmentation result of a right lung with pathological thick fissures.

2.2 Segmentation

The actual segmentation of the lung into its lobes is achieved by computing an approximate solution, which is then refined by minimizing an energy equation that contains information on the lung structures computed in section 2.1.

2.2.1 Approximate Lobe Segmentation

An approximate lung lobe segmentation S_A can be obtained with the help of the airway tree. This is achieved by taking the lobe based airway segmentation and computing a distance map on it. Voxels are then assigned labels I_p according to their nearest airway branch. This approach is leading to solutions in good approximation, as the airway branches are typically centered in the lobes. Figure 3 on the right shows an approximate lobe segmentation of a right lung as overlay to the original CT image. On the left in figure 3 the corresponding airway segmentation can be seen.

2.2.2 Energy Equation

The anatomical structures that are described in section 2.1 are combined in an energy equation of the form:

$$E(f) = \sum_{p,q \in N} V_{p,q}(f_p, f_q) + \sum_{p \in P} D_p(f_p) \qquad (4)$$

In (4) the binary term $V_{p,q}$ is defining the energy that is added to the system by two neighboring voxels p and q with labels f_p and f_q. It is therefore often referred to as interaction term. The unary term D_p
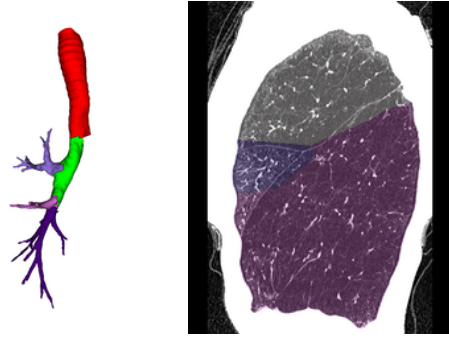

Figure 3: Left: Airway segmentation of a right lung; Right: CT image (sagittal slice) of the same lung with the approximate lobe labelling shown as overlay; the voxels are assigned labels corresponding to their nearest airway branch.

defines the energy for assigning a single voxel p the value f_p.

The minimization of (4) is consequently leading to an optimal lobe segmentation. Boykov et al. showed that the problem of minimizing energy equations of the form presented in (4) is often very difficult and finding the optimal solution is NP-hard (Boykov et al., 2001). In the same work an algorithm ($\alpha - expansion$) for finding a local minimum within a known factor to the global minimum is presented. The α-expansion algorithm is based on the computation of graph cuts. The cut separates or segments the vertices of the graph into a set of α and $\overline{\alpha}$ vertices. The graph is constructed in a way that α can only expand. By iterating over all labels and setting α to the current label it is possible to find solutions for images with multiple labels. The cost of the graph cut represents the energy of the system. Thus, only the solutions that undercut the current lowest solution are kept in the iteration process. If the algorithm converges, it is stopped.

The energy equation we propose for the lobe segmentation using the anatomical structures of section 2.1 is given by (4) where the binary term $V_{p,q}$ is shown in (5) and the unary term D_p in (6).

$$V_{p,q}(f_p, f_q) = k_{f_b} \cdot P(a, b) \qquad (5)$$

$$D_p(f_p) = 0 \quad \text{if} \quad f_p = I_p \\ = 1.0 \cdot k_f \cdot k_v \cdot k_a \quad \text{if} \quad f_p \neq I_p \qquad (6)$$

The unary term D_p is set to 0 if the value f_p of voxel p equals the value I_p in the approximate lobe segmentation S_A. Doing so the system is constrained to stay relatively close to S_A. The anatomical information retrieved from the lung structures are
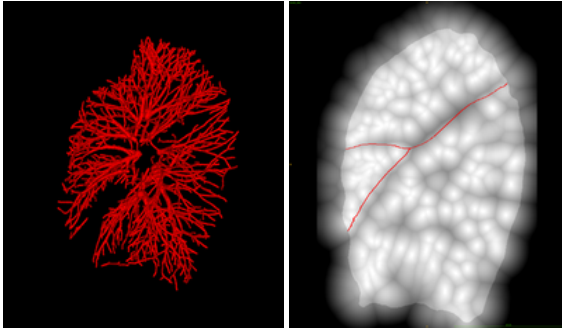
Figure 4: Left: Vasculature of a right lung. The lobe boundaries can be guessed from regions devoid of vessels. Right: An inverted distance map computed on the vasculature. Dark regions denote regions with high fissure probability. The real boundary is displayed as overlay.

incorporated into the unary term by the parameters k_f, k_v and k_a if $f_p \neq I_p$.

The fissures are integrated by the parameter k_f, which equals to 0 if $p \in F$ and otherwise to 1. This implies that voxels that are part of fissures are equally likely assigned to each label.

k_v is a parameter to include information retrieved from the lung vessels. A distance map is computed based on the vessels. This distance map is inverted and scaled to a range of $[0,1]$. Voxels with a large distance to the vessels have values close to 0, while voxels part of the vessels have values of 1. Figure 4 on the left shows a vessel tree of a right lung. The corresponding distance map is visualised on the right. The true boundary is shown as an overlay on the distance map.

The airway tree is considered by the third parameter (k_a) in (6). Two considerations regarding the airways are made. First we assume that the accuracy of the approximate lobe segmentation S_A is higher in regions that are in close proximity to the airways. With increasing distance to the airways the certainty for the correctness of the label for a given voxel decreases. This property is represented by the parameter k_{a_d}. The second consideration about the airways is done regarding the relative distance between the two nearest airway branches to the current voxel. If a voxel is close to one branch and relatively far away from the second nearest branch, then the certainty that this voxel is assigned the right label is increased. However, if a voxel lies almost inbetween two branches the certainty is decreased. This property is represented by the parameter k_{a_r}. The two parameters for the airways are combined to $k_a = k_{a_d} \cdot k_{a_r}$.

$P(a,b)$ in the binary term in (5) refers to the Potts model (Wu, 1982). $P(a,b) = k_p$ if $a \neq b$ and 0 oth-

erwise. By using the Potts model in the binary term the system is pushed towards solutions with closed structures and smooth boundaries. To favour segmentations with boundaries on the fissures we include a factor k_{f_b}. This factor is always 1 except for voxels that are part of the fissures, in which case $k_{f_b} = 0$. Therefore, boundaries on the fissures are more likely to occur as they do not increase the energy. In regions where no fissures are detected by the fissure segmentation algorithm presented in section 2.1.4, the Potts model leads to smooth interpolations of the indistinct boundaries between the lung lobes.

3 EXPERIMENTS AND RESULTS

Two different experiments using two distinct datasets were conducted.

3.1 Experiment 1

The first experiment was realised using a dataset of 25 CT images. Two independent and unbiased individuals who had been adequately trained and not been part of the development of the algorithm, manually placed approximately 500 markers along the fissures. Distinct markers were set for each fissure making an individual evaluation for the left oblique, right oblique and right horizontal fissure possible. Distances between the manually placed markers on the fissures and the closest lobe boundary in the segmentation were determined as measure of segmentation accuracy. The distances were measured as positive and negative depending on the relative position of the markers and the boundary resulting from the automatic lobe segmentation. Regarding the left lung this led to positive distances for markers that are part of the lower lobe in the automatic segmentation and negative results for markers that are part of the upper lobe. Considering the right lung negative values were either used for markers of the horizontal fissure that were not part of the middle lobe in the segmentation or markers of the oblique fissure that were not part of the lower lobe.

Two out of a total of 25 CT images had been excluded because of undefined fissures in the image and failing bronchus labelling, respectively. In two further scans, no markers had been set for the right horizontal fissure as it was not visible in the CT scans.

Using this evaluation protocol the median distance was 0.00mm (interquartile range: -0.86-0.00mm). The right and left oblique fissures median distances were 0.00mm (0.00-0.80mm) and 0.00mm (-0.86-0.00mm), respectively. The median distance for the right horizontal fissure was 0.00mm (-1.05-0.00mm).

The results for each individual case are visualised in figure 5.

Using the same evaluation protocol with absolute distances, the median distance was 1.04mm (0.88-1.09mm). The right and left oblique fissures median distances were 0.95mm (0.87-1.06mm) and 0.93mm (0.87-1.05mm), respectively. The median distance for the right horizontal fissure was 1.06mm (1.03-1.09mm).

In figure 6 on the left, a lung lobe segmentation result for a left lung can be seen. On the right of figure 6 the result for the corresponding right lung is shown.

3.2 Experiment 2

Experiment 2 was conducted on the LObe and Lung Analysis challenge (LOLA11) data set, which contains 55 CT images from different clinically common scanners and protocols. It includes many cases with severe pathologies, which makes a segmentation challenging for automatic algorithms. In cases where the airway segmentation failed or produced results containing missing airway branches with respect to the lobes, a manual correction had been performed. A quantitative (see table 1) as well as a qualitative evaluation, by visual inspection, of the segmentation results on the LOLA11 dataset shows promising results even on pathological lungs.

Figure 7 shows the results for the left and right lung of case 42. Even though the left lung contains focal regions of emphysema, the result shows a very precise segmentation. The result for the right lung shows a good segmentation even in regions where the oblique fissure is incomplete.

On the right in figure 8 the segmentation result for the right lung of case 13 is visualised. It shows the slice of the same right lung shown in figure 3. Starting from the initial segmentation in figure 3 the final result follows perfectly the fissures. On the left in figure 8 the result for the left lung of case 1 is shown.

Two different challenging cases regarding the lobe segmentation are shown in figure 9. On the left, the left lung of case 6 is shown. The lung shows an example for lung fibrosis together with regions of emphysema and a bulla. Due to these severe pathologies, the upper lobe is uncommonly small. In conjunction with a poor airway segmentation this leads to an approximate lobe segmentation that is far away from the optimal, thus resulting in a weak segmentation of the pulmonary lobes. On the right the result for the right lung of case 54 is shown. While the segmentation is very precise with respect to the right oblique fissure, the segmentation of the middle lobe is not correct. This can be explained by a weak approximate segmenta-

Table 1: Results of lobe segmentation for the 55 scans in the LOLA11 challenge.

	LU	LL	RU	RM	RL
mean	0.929	0.884	0.873	0.714	0.928
SD	0.118	0.231	0.169	0.322	0.104
min	0.272	0	0	0	0.341
Q1	0.922	0.919	0.853	0.575	0.909
median	0.971	0.965	0.938	0.863	0.973
Q3	0.991	0.983	0.977	0.941	0.983
max	0.997	0.993	0.996	0.994	0.995
score:	0.866				

tion, which was derived from an already weak airway segmentation.

With a score of 0.866, our algorithm performs in the range of the other state-of-the-art methods. Merely the interactive approaches show distinctly better results (LOLA11, 2017). Detailed comparisons to other methods are difficult to perform, as labelled datasets for lobe segmentation are not publicly available.

4 CONCLUSION AND FUTURE WORK

In this paper, we have proposed a new algorithm for fully automatic lung lobe segmentation using α-expansion. This approach allows to combine anatomical structures, derived from the original CT image, as well as prior knowledge on the shape of lung lobes into an energy equation. The Potts model is used as prior knowledge, which is leading to smooth lobar surfaces. An initial approximation to the lung lobe segmentation, close to the actual segmentation, is first derived by computing a distance map on the labelled airway segmentation. The multiscale fissure segmentation approach is drastically improving the amount of detected fissures while simultaneously increasing the amount of spuriously detected structures. False positives in the fissure segmentation are however no issue regarding the final lobe segmentation as the system stays close to the initial approximation. Thus finding a good approximation is important to achieve good results, which is evident from the observation that a poor segmentation is almost always attributable to a weak approximate lobe segmentation.

While limitations in our method are seen in the airway and lung segmentation steps, which consist of the combination of two algorithms to yield robust results, the approach of minimizing the devised energy equation has shown good results for lobe segmentation in our experiments.
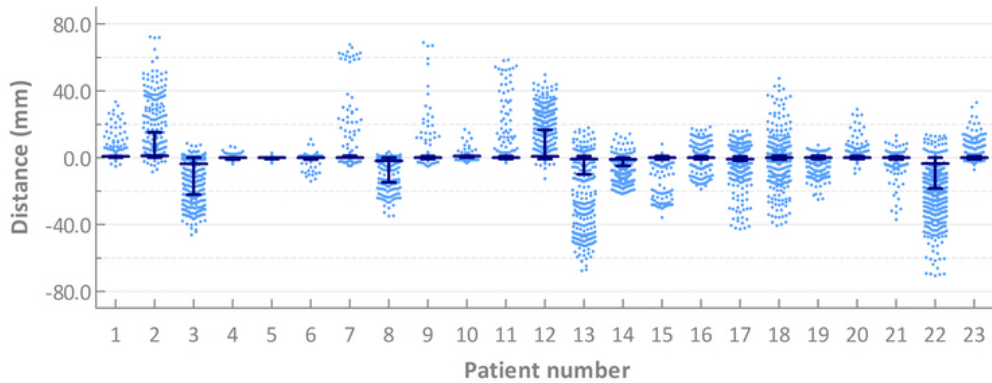
Figure 5: Distances of the individual markers from the nearest automatically detected fissure for each patient in experiment 1.
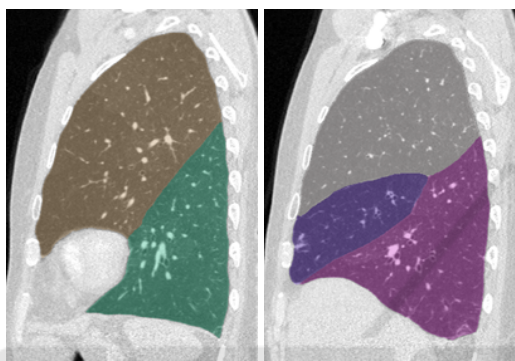

Figure 6: Example for a segmentation result of a left lung (left) and a right lung (right) a patient from experiment 1.
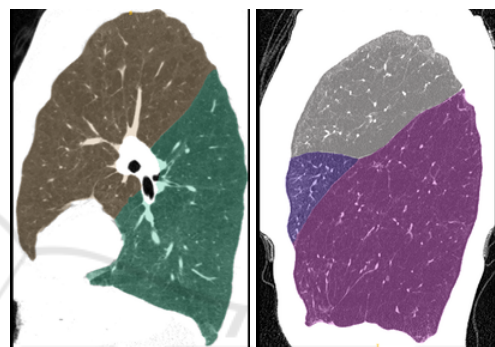

Figure 8: Left: Segmentation result for the left lung of LOLA11 case 1. Right: Segmentation result for the right lung of LOLA11 case 13.
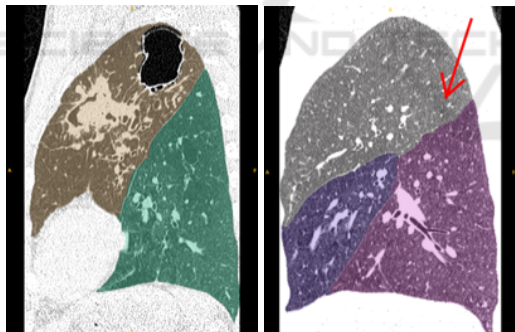

Figure 7: Segmentation results for LOLA11 case 42. Note the invisible fissure (arrow).
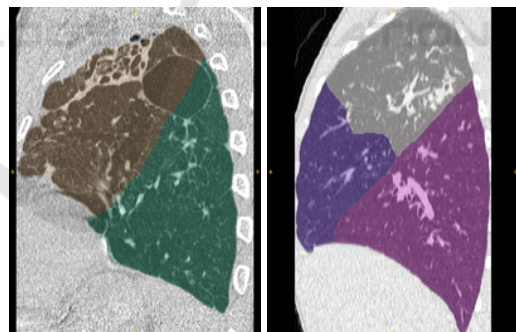

Figure 9: Left: Segmentation result for the left lung of LOLA11 case 6. Right: Segmentation result for the right lung of LOLA11 case 54.

With this work we established a general method with modular components as suggested in (Doel et al., 2015). Future work will consist of gradually improving the individual modules for lung, vessel, fissure and especially airway segmentation.

ACKNOWLEDGEMENTS

REFERENCES

Aziz, A., Ashizawa, K., Nagaoki, K., and Hayashi, K. (2004). High resolution CT anatomy of the pulmonary fissures. *Journal of thoracic imaging*, 19(3):186–191.

Benmansour, F., Türetken, E., and Fua, P. (2013). Tubular geodesics using oriented flux: An ITK implementation. *The Insight Journal*.

Boykov, Y., Veksler, O., and Zabih, R. (2001). Fast approximate energy minimization via graph cuts. *IEEE*

Transactions on pattern analysis and machine intelligence, 23(11):1222–1239.

Bragman, F. J., McClelland, J. R., Jacob, J., Hurst, J. R., and Hawkes, D. J. (2017). Pulmonary lobe segmentation with probabilistic segmentation of the fissures and a groupwise fissure prior. *IEEE Transactions on medical imaging*, 36(8):1650–1663.

Doel, T., Gavaghan, D. J., and Grau, V. (2015). Review of automatic pulmonary lobe segmentation methods from CT. *Computerized Medical Imaging and Graphics*, 40:13–29.

Doel, T., Matin, T. N., Gleeson, F. V., Gavaghan, D. J., and Grau, V. (2012). Pulmonary lobe segmentation from CT images using fissureness, airways, vessels and multilevel B-splines. In *9th IEEE International Symposium on Biomedical Imaging (ISBI), 2012*, pages 1491–1494. IEEE.

Frangi, A. F., Niessen, W. J., Vincken, K. L., and Viergever, M. A. (1998). Multiscale vessel enhancement filtering. In *International Conference on Medical Image Computing and Computer-Assisted Intervention*, pages 130–137. Springer.

Gu, S., Wang, Z., Siegfried, J. M., Wilson, D., Bigbee, W. L., and Pu, J. (2012). Automated lobe-based airway labeling. *Journal of Biomedical Imaging*, 2012:1.

Hayashi, K., Aziz, A., Ashizawa, K., Hayashi, H., Nagaoki, K., and Otsuji, H. (2001). Radiographic and CT appearances of the major fissures. *Radiographics*, 21(4):861–874.

Helmberger, M., Pienn, M., Urschler, M., Kullnig, P., Stollberger, R., Kovacs, G., Olschewski, A., Olschewski, H., and Bálint, Z. (2014). Quantification of tortuosity and fractal dimension of the lung vessels in pulmonary hypertension patients. *PloS one*, 9(1):e87515.

Lassen, B., van Rikxoort, E. M., Schmidt, M., Kerkstra, S., van Ginneken, B., and Kuhnigk, J.-M. (2013). Automatic segmentation of the pulmonary lobes from chest CT scans based on fissures, vessels, and bronchi. *IEEE Transactions on medical imaging*, 32(2):210–222.

Lassen-Schmidt, B. C., Kuhnigk, J.-M., Konrad, O., van Ginneken, B., and van Rikxoort, E. M. (2017). Fast interactive segmentation of the pulmonary lobes from thoracic computed tomography data. *Physics in Medicine and Biology*, 62(16):6649.

Law, M. W. K. and Chung, A. C. S. (2008). *Three Dimensional Curvilinear Structure Detection Using Optimally Oriented Flux*, pages 368–382. Springer Berlin Heidelberg, Berlin, Heidelberg.

LOLA11 (2017). [Online; accessed 30-October-2017].

Otsu, N. (1979). A threshold selection method from gray-level histograms. *IEEE Transactions on systems, man, and cybernetics*, 9(1):62–66.

Payer, C., Pienn, M., Bálint, Z., Shekhovtsov, A., Talakic, E., Nagy, E., Olschewski, A., Olschewski, H., and Urschler, M. (2016). Automated integer programming based separation of arteries and veins from thoracic CT images. *Medical image analysis*, 34:109–122.

San Jose Estepar, R., Ross, J. C., Harmouche, R., Onieva, J., Diaz, A. A., and Washko, G. R. (2015). Chest imaging platform: an open-source library and workstation for quantitative chest imaging. In *C66. Lung imaging II: New probes and emerging technologies*, pages A4975–A4975. Am Thoracic Soc.

Schuhmann, M., Raffy, P., Yin, Y., Gompelmann, D., Oguz, I., Eberhardt, R., Hornberg, D., Heussel, C. P., Wood, S., and Herth, F. J. (2015). Computed tomography predictors of response to endobronchial valve lung reduction treatment. comparison with chartis. *American journal of respiratory and critical care medicine*, 191(7):767–774.

Tanabe, N., Muro, S., Tanaka, S., Sato, S., Oguma, T., Kiyokawa, H., Takahashi, T., Kinose, D., Hoshino, Y., Kubo, T., Ogawa, E., Hirai, T., and Mishima, M. (2012). Emphysema distribution and annual changes in pulmonary function in male patients with chronic obstructive pulmonary disease. *Respiratory research*, 13(1):31.

Van Rikxoort, E. M., Prokop, M., de Hoop, B., Viergever, M. A., Pluim, J. P., and van Ginneken, B. (2010). Automatic segmentation of pulmonary lobes robust against incomplete fissures. *IEEE Transactions on medical imaging*, 29(6):1286–1296.

Weder, W., Thurnheer, R., Stammberger, U., Bürge, M., Russi, E. W., and Bloch, K. E. (1997). Radiologic emphysema morphology is associated with outcome after surgical lung volume reduction. *The Annals of thoracic surgery*, 64(2):313–320.

Wu, F. Y. (1982). The Potts model. *Reviews of Modern Physics*, 54:235–268.

Zhang, L., Hoffman, E. A., and Reinhardt, J. M. (2006). Atlas-driven lung lobe segmentation in volumetric X-ray CT images. *IEEE Transactions on medical imaging*, 25(1):1–16.